

Intelligent Tire-Based Slip Ratio Estimation Using Different Machine Learning Algorithms

Nan Xu, Zepeng Tang, Jianfeng Zhou, Hassan Askari

Abstract—Estimation of the longitudinal slip ratio of tires is important in boosting the control performance of the vehicle under driving and braking conditions. In this paper, the slip ratio is estimated using four machine learning algorithms (Neural Network, Gradient Boosting Machine, Random Forest and Support Vector Machine) based on the acceleration signals from the tri-axial MEMS accelerometers utilized in the intelligent tire system. The experimental data are collected through the MTS experimental platform. The corresponding acceleration signals within the tire contact patch are extracted after filtering to be used for the training the aforesaid machine learning algorithms. A comparison is provided between the implemented ML algorithms using a 10-fold CV. NRMS errors in the CV results indicate that NN has the highest accuracy in comparison with other techniques. The NRMS errors of NN, GBM, RF, and SVM are 2.59%, 3.30%, 4.21%, and 5.34%, respectively. Among these techniques, GBM has a more stable results as it has the smallest output variance. The present study with the fusion of intelligent tire system and machine learning algorithms paves the way for the accurate estimation of tire slip ratio, which is critical for the development of reliable vehicle control algorithms.

Index Terms—Intelligent tire, tire slip ratio estimation, machine learning, vehicle system dynamics, sensing systems.

I. INTRODUCTION

SEVERAL vehicle control systems have been developed over the years such as Traction Control System (TCS) [1], Anti-lock Braking System (ABS) [2], and Electronic Stability Program (ESP) [3]. The purpose of these systems is to stabilize the vehicle within a reasonable safety range by changing the forces between the tires and the road when the vehicle becomes uncontrollable. For example, to ensure that the tire forces are within the limits of adhesion, ABS is activated to maintain the tire longitudinal forces around the maximum adhesion by controlling the tire slip ratio within the optimal range. Considering the rapid development of electric vehicle in recent years, it is expected to witness novel vehicle control systems. The demand of novel control strategy is even more pronounced because of fast response capability of electric motors. Due to this characteristic of electric motors, tires are more prone to slip and spin, specially at the start of driving. This leads to extra energy consumption resulting in lower drivability range and environmental issues[4]. Furthermore, electric vehicles directly control output torque of motor and its

relation with tire forces. However, this is beneficial for having a more robust control over tire forces, its fast response can cause new issues as it needs faster and more accurate vehicle and tire states estimation. In fact, the better performance of electric vehicle control depends on the faster and more accurate estimation of tire parameters, especially the slip ratio.

Traditional slip ratio estimation methods are generally divided into two main categories. The first one uses the vehicle velocity (V) and wheel angular velocity (V_w) to directly calculate the slip ratio [5], [6], [7], [8], [9], [2]. The second category estimates tire slip ratio without using the vehicle velocity[10], [11], [7], [12], [13], [14]. The mathematical definition of slip ratio (κ) is shown in Equation 1. In terms of physical meaning, slip ratio is defined as the skidding level of the tire against the road. The corresponding tire model is shown in Figure 1.

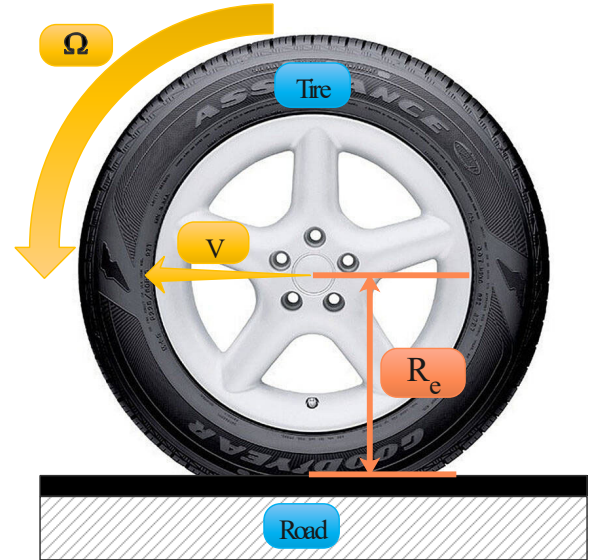


Fig. 1: Schematic representation of a tire interacting with road

$$\kappa = \frac{V_w - V}{\max|V_w, V|} = \frac{\Omega R_e - V}{\max|\Omega R_e, V|} \times 100\% \quad (1)$$

where V_w and V are wheel velocity and vehicle velocity, respectively. Ω is wheel angular velocity and R_e is the tire effective radius.

Fujimoto et al. [14] proposed the technique of tire slip ratio estimation without considering the vehicle speed. They developed the state space equation of slip ratio versus the angular velocity of the tires, and the driving torque of an

N. Xu, Z. Tang and J. Zhou are with the State Key Laboratory of Automotive Simulation and Control, Jilin University, Changchun, Jilin, 130025, China and N. Xu is also with the Department of Mechanical and Mechatronics Engineering, University of Waterloo, ON. N2L3G1, Canada, e-mail: (xunan@jlu.edu.cn, tangzp19@mails.jlu.edu.cn, and zhoujf20@mails.jlu.edu.cn).

H. Askari is at the Department of Mechanical and Mechatronics Engineering, University of Waterloo, ON. N2L3G1, Canada e-mail: (h2askari@uwaterloo.ca, and a.khajepour@uwaterloo.ca)

electric vehicle. This driving torque can be measured by the current in the motor. The same method was then used in [11].

Researchers have also used accelerometers to obtain vehicle acceleration signals to be combined with wheel velocity for the slip ratio estimation [10], [12]. M. Boisvert et al. [7] have developed a non-linear equation to mathematically show the relation of slip ratio and motor torque. Based on their proposed formulation, the slip ratio can be estimated directly based on the motor torque.

The popular slip ratio estimation technique relies on the vehicle speed and the wheel velocity. However, accurate estimation of vehicle speed has always been a concern for researchers in the area of vehicle dynamics [15], [16], [17]. Moreover, autonomous driving has recently attracted the attention of researchers as well as automotive industries. Therefore, it is highly needed to estimate vehicle speed with higher accuracy, especially in path planning, driving, and braking on high-precision maps. Researchers have tried other approaches to estimate the vehicle speed, such as using acceleration signals obtained from accelerometers installed on the vehicle, or using Kalman observers to establish the states equation related to the vehicle speed [15]. It shows that the most of slip ratio estimation methods are dependent on the results of vehicle speed estimation. Accordingly, we can also assume an opposite case, if it is possible to estimate the slip ratio accurately by being able to estimate it without using the vehicle speed signal, then the vehicle speed is calculated backwards from the precise slip ratio estimate, which provides a new possibility for the vehicle speed estimation.

As the state-of-the-art shows, the intelligent tire system has not been used for the estimation of tire slip ratio, which is the scope of the present research. Tire contact patch characteristics are important for understanding the study of vehicle dynamics [18], [19]. The tire forces, slip angle, and slip ratio generated by the tire-road interaction are reflected within the contact patch. The intelligent tire system is a direct and reliable approach to obtain real-time information about the tire contact patch with the use of embedded sensory systems inside the tire [20]. Very recently, researchers have implemented intelligent tire system for online estimation of tire forces and tire slip angles with a high accuracy [21], [22]. The so-called intelligent tire system is a system that uses sensors (e.g., accelerometers [22], stress sensors [23], triboelectric nanogenerator (TENG) [24], [25], optical sensors [26], capacitive sensors [27], optical fiber sensors [28], surface acoustic wave sensors [29], magnetic sensors [30], and ultrasonic distance sensors [31]) inside the tire to measure the signals generated by the tire as it enters and leaves the contact patch for further processing. The so-called intelligent tire system is a system that uses sensors (e.g., accelerometers [22], stress sensors [23], triboelectric nanogenerator (TENG) [24], [25], optical sensors [26], capacitive sensors [27], optical fiber sensors [28], surface acoustic wave sensors [29], magnetic sensors [30], and ultrasonic distance sensors [31]) inside the tire to measure the signals generated by the tire as it enters and leaves the contact patch for further processing.

As opposed to the state imposed on the tire from the outside, the information is actively obtained by the sensors inside the

tire, allowing the tire to offer its own state parameters to the outside, which is called "intelligent" tire. Combining the authors' review of the merits and demerits of the different sensors used in intelligent tires in [32] and the authors' estimation of the effectiveness of tire force, slip angle estimation in [21], [22]. Accelerometer is currently the most popular sensors used in intelligent tire systems. So it's also applied in this research work for slip ratio estimation.

In this paper, firstly, the intelligent tire system is designed by gluing the accelerometer in the inner liner of the tire, and when the tire rotates, the value of the accelerometer changes when it enters and leaves the contact patch. The signal is then collected by a data acquisition device using a high sampling frequency for subsequent analysis and processing. During the data analysis, two attractive features of the vertical acceleration signal are discovered, which are correlated with the slip ratio. Based on these features we employ four machine learning algorithms to model the relationship between the both. In order to make the algorithm more highly efficient, it is necessary to reduce the data points of the vertical acceleration signal, because the original signal sampling frequency is 10 kHz, which is a great task for the algorithm's operation with such large data. Through shrinking, it is finally determined that an acceleration sample point is extracted every 3.5 degrees in the 70-degree range of the tire contact patch. In other words, 20 sample points are used as the input of the machine learning algorithm for each rotation of the tire. In addition, for a more adequate research comparison, the wheel angular velocity (Ω) is also taken into account and combined with the vertical acceleration signal as the input to the machine learning algorithm. The results of the slip ratio estimation of the two input types using only the vertical acceleration as input vs. the combination of both wheel angular velocity and vertical acceleration as input, whose the latter is found to have less estimation error and are more stable. Finally, the models of four machine learning algorithms, Neural Network (NN), Gradient Boosting Machine (GBM), Random Forest (RF), and Support Vector Machine (SVM), are evaluated using wheel angular velocity and vertical acceleration as algorithm inputs, respectively.

The framework of this paper is organized as follows. Section II introduces the test system as well as the design of the working conditions, where the test system includes the MTS test system and the intelligent tire system. Section III analyzes the acceleration signal to extract the features related to the slip ratio. Section IV presents the pre-processing of the data to prepare for the modeling of the machine learning algorithms. Section V comprehensively analyzes and discusses the estimation results of the machine learning algorithms using two input types for the slip ratio, respectively, and provides a complete evaluation of the four algorithms. Finally, the conclusions and future research work of this paper are stated.

II. TEST AND SIGNAL ACQUISITION

The entire test system can be regarded as two systems, which are the Measure Test Simulate (MTS) tire test system and the intelligent tire system. The MTS tire test system is

used to set up different scenarios and collect data such as slip ratio, slip angle, tire force, etc., while collecting acceleration sensor signals based on the intelligent tire system. The whole test system is shown in Figure 2, and the details of which are presented in this section.

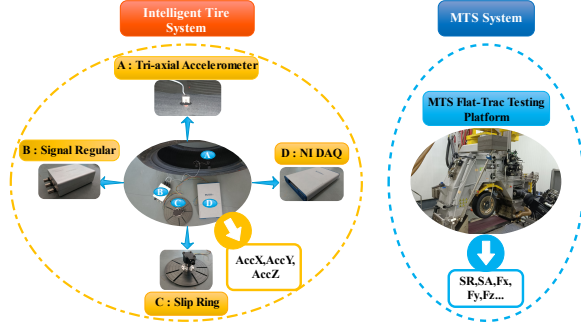


Fig. 2: The entire test system

A. MTS Tire Experimental System

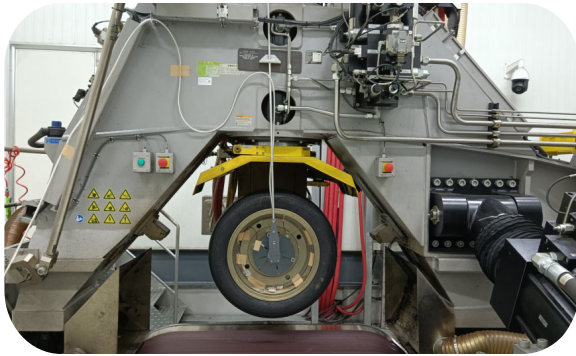


Fig. 3: MTS tire testing platform

To get the data with different slip ratio, the MTS Flat-Trac testing system (Fig. 3) is applied to conduct numerous experiments. Two types of data are collected in the operation, one from the MTS test bed, including slip ratio (SR, which is same as the previously mentioned κ), tire force, slip angle and wheel angular velocity (Ω), and the other from the acceleration sensors, which are longitudinal, lateral and vertical acceleration signals (named as $AccX$, $AccY$, and $AccZ$).

B. Intelligent Tire System

The intelligent tire system in this article consists of a Micro-electro mechanical Systems (MEMS) tri-axial acceleration sensor, a high-speed slip ring, a signal regulator, and an National Instrument (NI) data acquisition system (DAQ), as shown in Fig. 2.

The tri-axial acceleration sensor is glued the inner liner of the tire to measure the $AccX$, $AccY$ and $AccZ$ acceleration signals generated within the tire's contact patch in Fig. 4a, and the definition of its coordinates system orientation is shown in Fig. 4b. The signal wire then passes through the valve nozzle through the rim, see Fig. 5a, where the valve nozzle device is sealed with sealant to avoid tire air leakage. After

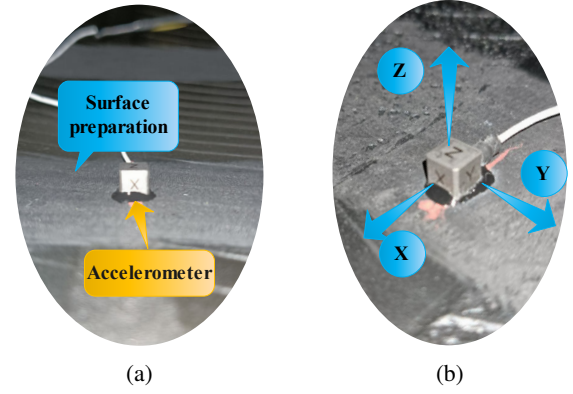


Fig. 4: (a). Installation of accelerometer in tire; (b). Coordinate system of accelerometer in tire

TABLE I: Testing Scenarios

| Driving/Braking | Parameters |
|-------------------|---|
| Tire Model | BridgeStone 215/55R17 |
| Pressure [kPa] | 250 |
| Vertical Load [N] | 2680, 4020, 5360 |
| Velocity [km/h] | 30, 60 |
| Slip Ratio [%] | $\pm 4, \pm 3, \pm 2, \pm 1$, Triangular Wave (3% and up to 30%) |

exiting the rim, it has to pass through the high-speed slip ring in Fig. 5b, this is a 6-channel slip ring made by Michigan Scientific, which is designed to be mounted on the rim and used to transmit the acceleration signal from the rotating tire to the NI DAQ system. The signal regulator uses three channels (corresponding to the three acceleration directions) to provide a constant current source to supply power the accelerometer. The NI DAQ system can be used to collect the acceleration signal by adjusting the signal channels, sampling frequency and sampling method (differential mode or single-ended reference mode). The single-ended reference mode (selected when the signal regulator is grounded) is adopted for this test, and the sampling frequency is chosen to be 10 KHz, which is adequate to meet the research requirements.

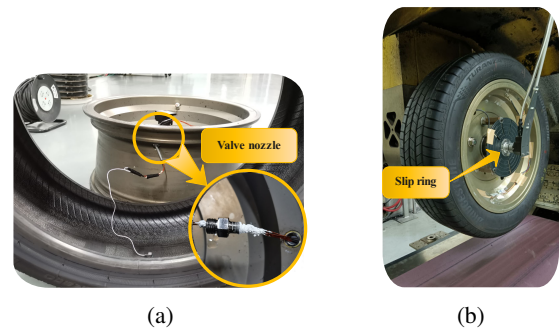


Fig. 5: Transmission method of signal line (a. Using the valve nozzle across the rim; b. Transferred via slip ring)

C. Test Scenarios

This experiment is conducted using Bridgestone tires for testing, and three loads, two velocities and different slip

ratios are changed respectively. There are two main types according to the variation of the slip ratio, one is the step slip ratio change, which increases from -4% to +4% one by one, this condition can be noted as SSR. The other is the continuous triangular wave variation, a part of which is the small continuous slip ratio (SCSR), its alteration follows the 0-3%-3%-0 rule, and the remaining part is the large continuous slip ratio, the varying law is 0-30%-30%-0, which is named LCSR.

III. DATA ANALYSIS

In this section, the characteristics of the $AccZ$ signals at varying slip ratio are mainly observed. The reason why the $AccZ$ signal is chosen as the object of study for the longitudinal slip condition is that it has more distinct and regular characteristic, which are introduced in the following paragraphs. Figs. 6-7 show the $AccZ$ signals for different slip ratios in the range of tire contact patch (whose contact patch searching method is expanded in the next section). As described in the previous section, the data acquisition frequency is 10 kHz, and the $AccZ$ at varying slip ratio is shown in Figs. 6-7 after using 400 Hz Butterworth low-pass filtering here.

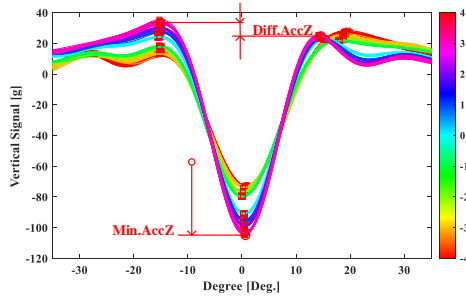


Fig. 6: Acceleration in time domain under step slip ratio (60km/h at 2680N load)

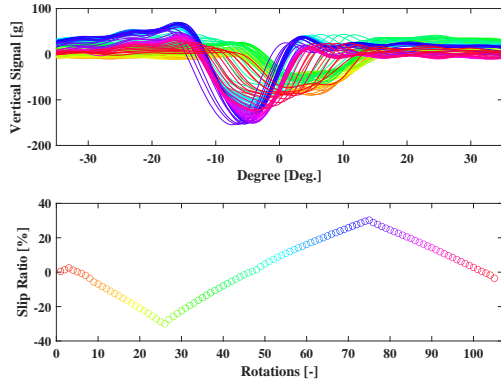


Fig. 7: Acceleration in time domain under triangular slip ratio (60km/h at 2680N load)

Figure 6 shows the $AccZ$ curves for the SSR condition at 60km/h-2680N, and the slip ratio variations are distinguished

by different colors as indicated in the legend on the right side of the figure. The pre-peak (left), the post-peak (right), and minimum value of the $AccZ$ curve are labelled by the boxes. In which the pre-peak and post-peak there is a difference, denoted $Dif.AccZ$. The peaks at the two sides of the $AccZ$ show low left and high right when the slip ratio is negative, and high left and low right when the slip ratio is positive. This feature is obviously different from the free rolling condition and the side slip condition [21], and is unique to the longitudinal slip condition. Its minimum value is recorded as $Min.AccZ$, which decreases gradually when the slip ratio changes from negative to positive.

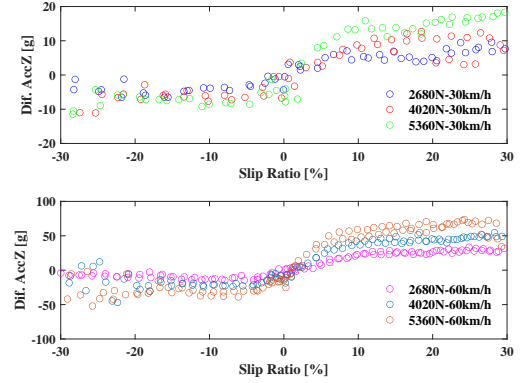


Fig. 8: Variation of $Dif.AccZ$ with slip ratio under different working conditions

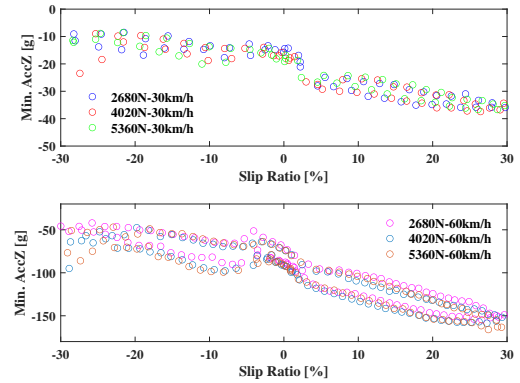


Fig. 9: Variation of $Min.AccZ$ with slip ratio under different working conditions

Figure 7 presents the vertical acceleration signal of the LCSR condition at 60 km/h-2680 N. From the figure, it can be seen that the variation of $Dif.AccZ$ and $Min.AccZ$ is the same as in SSR. Except that there is a more significant feature that the vertical acceleration signal is shifted overall with the change of slip ratio. To be more specific, the vertical acceleration signal shifts to the right when the slip ratio is negative, while it shifts to the left when the slip ratio is positive. In order to better analyze the relationship between these two features and slip ratio, the feature values are calculated separately for different velocity and load conditions, as shown in Figures 8-9.

Each color corresponds to a set of velocity and load. Figs. 8-9 show the variation curves of the two characteristics values of $Dif.AccZ$ and $Min.AccZ$ at different slip ratios, respectively. A non-linear variation law is presented in Fig. 8, where it can be observed that $Dif.AccZ$ increases faster with slip ratio within $\pm 10\%$, and the growth rate of $Dif.AccZ$ gradually slows down when it exceeds 10%. This variation law is similar to the longitudinal tire force vs. slip ratio in the longitudinal characteristics of tires, and it may be caused by the elastic hysteresis inherent in the tire rubber material. At the same time, it can be found that the change in velocity has a greater effect on the $Dif.AccZ$ value, which can be understood by the fact that the tire centrifugal acceleration is proportional to the velocity. In Figure 9 the $Min.AccZ$ shows a linear variation with the slip ratio. The positive slip ratio indicates the drive condition, and it is obvious that the Min. value decreases when transitioning from the braking condition to the drive condition. At the same time, a hysteresis phenomenon can be seen in the curve.

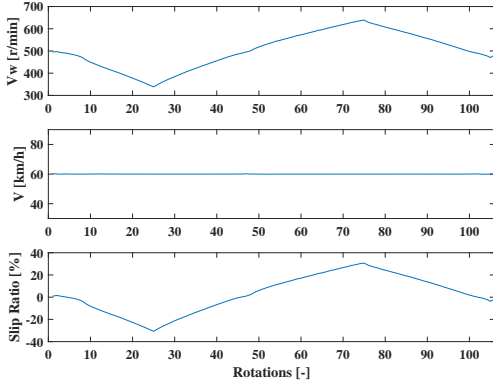


Fig. 10: Filtered wheel angular velocity signal

A promising correlation can be observed between these two features vs. the slip ratio above. However, it is difficult to parametrically perform modeling, so we tried to explore slip ratio estimation using machine learning methods. In addition, Ω is more available in current electric vehicles, and in order to more adequately investigate the contribution of the intelligent tire system, we put Ω and $AccZ$ together to as one of the inputs to the machine learning methods, in comparison with the results of training models using only $AccZ$. Figure 10 shows the Ω information acquired by the MTS test bed, which has been filtered so that it looks very smooth. The data pre-processing part is described below.

IV. METHODOLOGY

The most important part of machine learning algorithm is the pre-processing of data, and the pre-processing of data influences the result of the algorithm somewhat. In order to make the model simpler and more effective, the size of the data should be minimized as much as possible while ensuring its primary features. Meanwhile, the hyper-parameters of the machine learning algorithm used in this paper are described in detail below.

A. Data Pre-Processing

In the acceleration signal processing, the signal within the tire contact patch is of utmost importance. In the following, we will present how to extract the acceleration signal within the tire contact patch and select proper sample points within this range to provide the machine learning algorithm for training. The data pre-processing process is mainly divided into filtering, identifying the tire contact patch signal and extracting it, selecting the proper sample points, and data normalization. The whole process is as shown in flowchart 11.

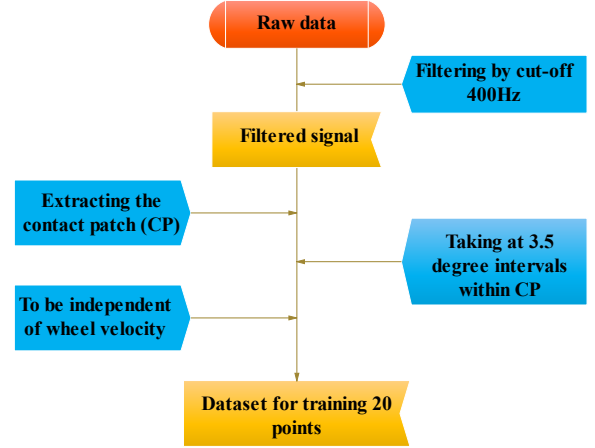


Fig. 11: Flowchart of data pre-processing

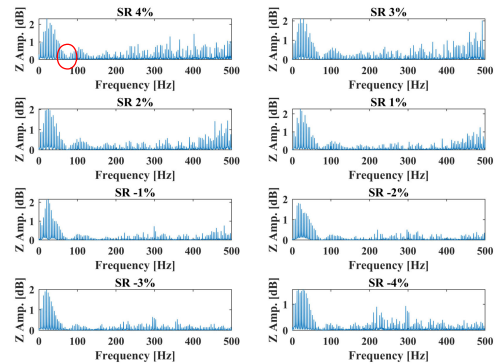


Fig. 12: Frequency spectrum analysis of $AccZ$ with different slip ratios under 30km/h

1) *Filtering*: The data acquired by the DAQ system at 10 kHz are sampled for spectrum analysis, and it can be seen from Figures 12 and 13 that the first peak cutoff frequencies (the location marked by the red circle in these figures) in the low frequency range of 30 km/h and 60 km/h are around 90 Hz and 150 Hz, respectively, in Fourier spectrum analysis of $AccZ$. It can also be observed that the change in slip ratio does not have a significant effect on the results of the spectral analysis of the vertical acceleration. It is only needed to select the maximum cutoff frequency (150Hz at 60km/h in Fig. 13) in the investigated working condition as the signal filtering cutoff frequency. but too low a cut-off frequency selection

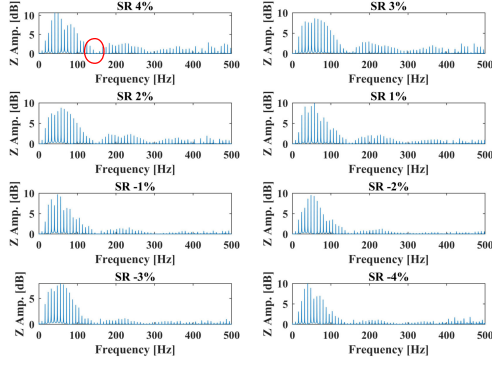


Fig. 13: Frequency spectrum analysis of $AccZ$ with different slip ratios under 60km/h

may result in the loss of features of the acceleration signal at certain frequencies within the tire contact patch, so 400 Hz is chosen here as the cut-off frequency for this study.

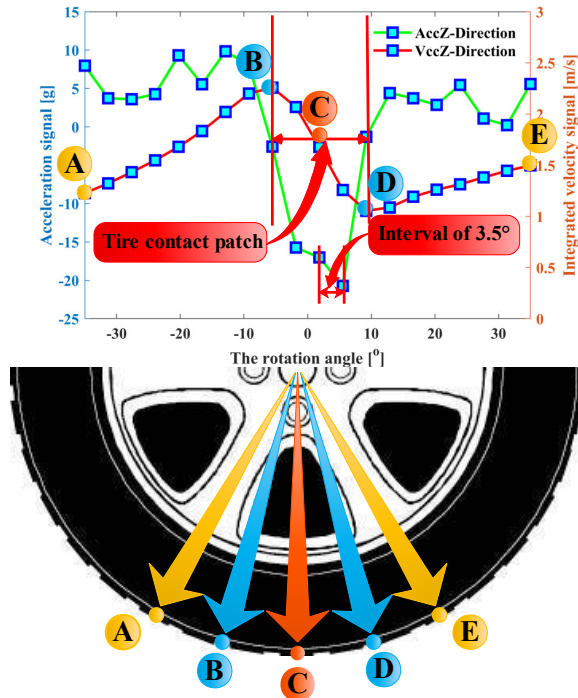


Fig. 14: Determining sample points within the contact patch

2) *Extracting the contact patch:* Due to the serious deformation of the longitudinal acceleration signal under longitudinal slip conditions, the method of determining the contact patch according to the front and rear peaks of the longitudinal acceleration is no longer applicable [22], and the integrated value of $AccZ$, i.e., the vertical velocity ($VccZ$), is used here to determine the contact patch. As shown in Fig. 14, it can be clearly seen that there are two peaks in the $VccZ$ when the sensor enters and leaves the contact patch. At the same time, the rotation angle of the tire is recorded by the encoder to accurately locate the position of the acceleration sensor.

The two peaks of the $VccZ$ (points B and D, respectively) are observed to correspond to about $\pm 10^\circ$ of the encoder, and the acceleration signal at $\pm 35^\circ$ is extracted in order to provide the machine learning algorithm with more information about the acceleration within the contact patch (it corresponds to points A and E). On the other hand, the number of sampling points changes with the increase of the wheel velocity, so it is also necessary to strip the effect caused by the velocity, and training samples can be captured according to the tire rotation angle. Meanwhile, in order to make the machine learning algorithm computationally efficient, a sample point is extracted at each 3.5° interval, while being able to ensure the acceleration information within the basic contact patch. That is, each rotation of the tire can generate 20 sample points to be utilized as input to the algorithm.

3) *Data normalization:* In order to enable the data to achieve fast convergence in machine learning algorithms, such as NN, GBM, and SVM, it is necessary to normalize the data, and the Min-Max normalization method is employed in this work as follows:

$$x_{norm} = \frac{x - x_{min}}{x_{max} - x_{min}} \quad (2)$$

where x presents the measured data, x_{min} and x_{max} are the minimum and maximum of the acquired data. However, RF does not require data normalization.

B. ML methods training

Within the field of state parameter estimation of vehicles and tires, the current predominantly used machine learning methods are Decision Tree algorithms (Decision Tree, Random Forest, Gradient Boosting Machine, etc.), Neural Network family (Artificial Neural Network, Convolutional Network, Recurrent Neural Network, etc.), and Support Vector Machine. And each single algorithm has its own pros and cons for all possible data sets, so in this paper, four commonly used algorithms, Artificial Neural Network, Gradient Boosting Machine, Random Forest, and Support Vector Machine are employed to investigate and evaluate the results of estimation of slip ratio.

NN mainly consist of an input layer, a hidden layer (one or more layers) and an output layer. It can obtain a deeper model representation by increasing the number of hidden layers. The NN based on the Rprop algorithm is used in this case because Rprop can effectively solve noise errors and is more suitable for hardware applications [33]. GBM is a method for regression and classification that combines weak learners into one strong learner by iterative methods [34]. Both RF and GBM belong to the class of decision trees, and compared to GBM, RF are easier to train and less prone to overfitting. In practical application, RF have proven to be a very effective method, but for processing regressions that do not go beyond the range of target values in which they are trained [35]. SVM can be used for classification and regression analysis. In solving the case of linearly indistinguishable data, it is achieved mainly by applying the kernel function technique, by mapping the vectors to a higher dimensional space, establishing a maximally interval hyperplane, and building two

critical hyperplanes parallel to each other on both sides of the hyperplane that separates the data, and the greater the distance between the two critical hyperplanes, the smaller the total error of the classifier [36].

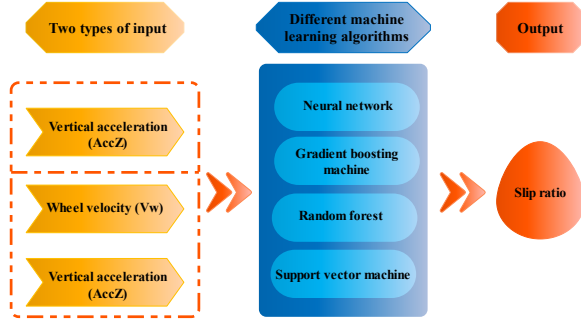


Fig. 15: Diagram of the input and output of different machine learning algorithms

Two categories are used as input to machine learning in this research, one with only $AccZ$ and the other with a combination of $AccZ$ and Ω . The output of both machine learning algorithms is the slip ratio, as shown in Figure 15. This research work is based on R software platform computing and uses four machine learning algorithms as a comparison analysis. The NN is based on the Rprop algorithm for slip ratio estimation, and its hidden layer is 10-5-1. The hyper-parameters of the GBM are as follows: trees = 4295, interaction.depth = 3, shrinkage = 0.1, n.minobinnode = 10, and bag.fraction = 1. The tree of RF is chosen to be 50. The gamma of SVM is set to 0.0312 and cost is 32. Two categories of inputs are used with the same hyper-parameters as above.

V. RESULTS AND DISCUSSIONS

This section is composed of three main parts. Firstly, the results of slip ratio estimation based on various machine learning algorithms with $AccZ$ as input are shown and expanded for three working conditions, which are SSR, SCSR and LCSR, respectively, and the three working conditions are assembled into a test set (AllCondi) for estimation. Next, the test results based on Ω and $AccZ$ as inputs are discussed. Finally, after analyzing and discussing, the estimation based on Ω and $AccZ$ as input is better, and in order to carry out more convincing evidence, the 10-fold CV method is invited for the final validation.

A. Different machine learning methods with $AccZ$

The $AccZ$ signal has a rather promising correlation with the slip ratio as described in the previous section, and also to consider the algorithm operation as simple as possible, it is only chosen as the input for machine learning for training. Figures 16-18 show the estimation results of the four machine learning algorithms for different operating conditions. For small slip ratio conditions such as SSR, SCSR, the estimation results are very satisfactory, as shown in Figs. 16 and 17. However, in the case of large slip ratio like LCSR, the estimation of all four machine learning algorithms will have

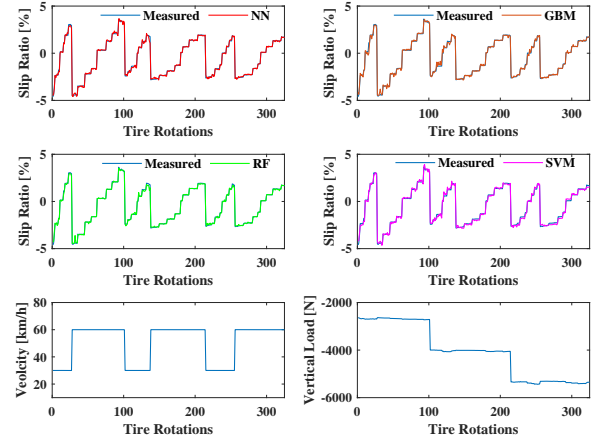


Fig. 16: Comparison of estimated SR with different ML methods under SSR using only $AccZ$

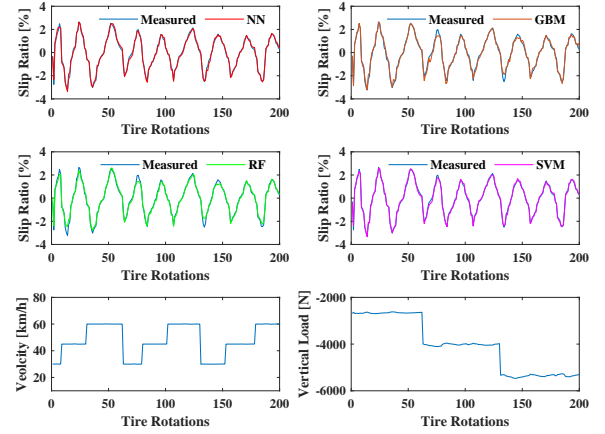


Fig. 17: Comparison of estimated SR with different ML methods under SCSR using only $AccZ$

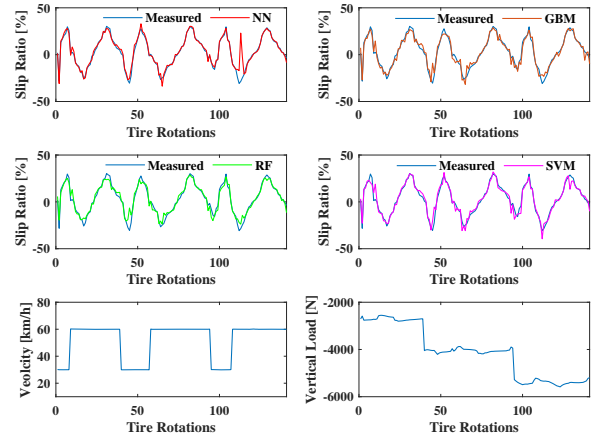


Fig. 18: Comparison of estimated SR with different ML methods under LCSR using only $AccZ$

some error at the sampling point around 120th in the figure 18, in which the error of NN algorithm is worse.

The estimation results of AllCondi, as seen in Figure 19, the errors are still mainly found in the areas with large slip ratios, especially for the RF and SVM methods. Figure

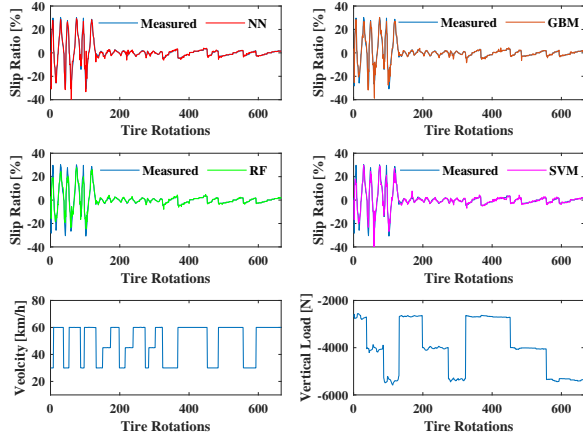


Fig. 19: Comparison of estimated SR with different ML methods under AllCondi using only $AccZ$

20 shows the training time for the training set of the four machine learning methods, the testing time for the test sets of different sub-working conditions, and the NRMS error results for their individual corresponding test sets, respectively. From the training time of the training set, GBM consumes more time among the four machine learning algorithms, then NN, and the time consumed by RF and SVM is almost equal. In terms of the test time for each sub-condition, GBM costs the most time regardless of which test set it is in. The last information that requires more attention is the NRMS error results. It can be observed from the figure that GBM has the most stable and outstanding performance in respect to the NRMS error, although it takes more time, whereas NN does not perform satisfactory in the test set with a large slip ratio like LCSR, for the same reason as observed in Figure 18, with a very large estimation error at the 120th sample point.

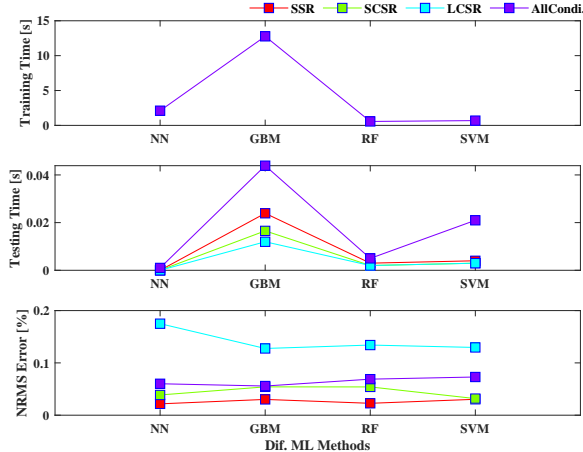


Fig. 20: Performance comparison of different ML methods using only $AccZ$

The results of the estimation based on Ω and $AccZ$ as input to the algorithm are analyzed in the following.

B. Different machine learning methods with $AccZ$ and Ω

The Ω is added to the $AccZ$ as the input to the machine learning algorithm, and the hyper-parameters within its algo-

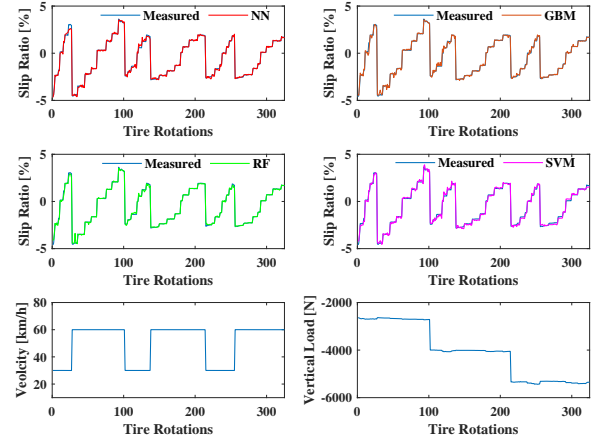


Fig. 21: Comparison of estimated SR with different ML methods under SSR using $AccZ$ and Ω

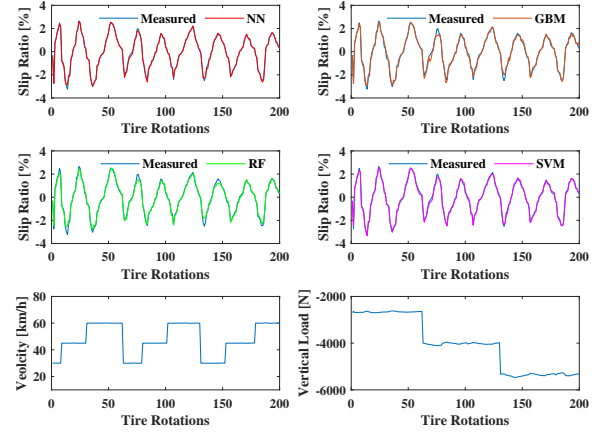


Fig. 22: Comparison of estimated SR with different ML methods under SCSR using $AccZ$ and Ω

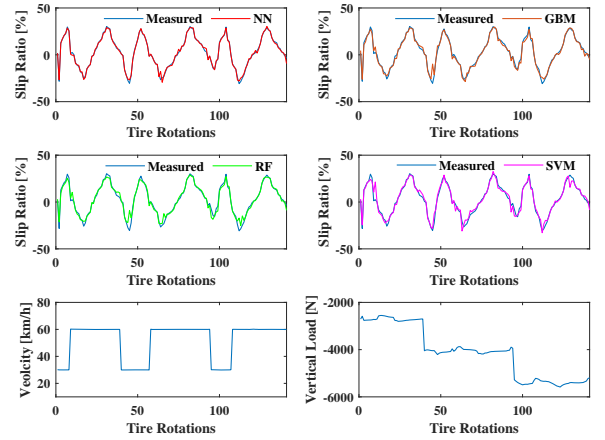


Fig. 23: Comparison of estimated SR with different ML methods under LCSR using $AccZ$ and Ω

rithm remain the same as before. Figures 21-23 show the estimation results for each sub-condition, focusing on the LCSR condition in Figure 23, where the error appearing at the 120th sample point of the previous subsection is greatly improved. This may be the result of the less prominent

characteristics of the *AccZ* here. Figure 24 shows the results of the AllCondi condition, which perform relatively well, except for some estimation errors in RF and SVM when large slip ratio occur. Figure 25 shows the training time, test time, and NRMS error respectively with Ω and *AccZ* as inputs. the time taken for training the models with different machine learning is different from before, NN takes a bit more time, but the results from NRMS error show that NN has superior results. In terms of testing time, SVM spends more time in testing AllCondi.

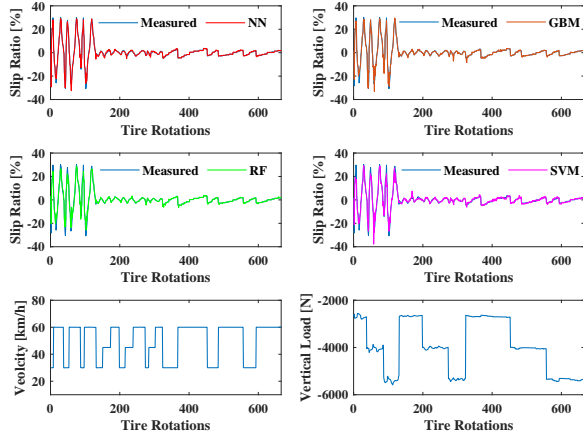


Fig. 24: Comparison of estimated SR with different ML methods under AllCondi using *AccZ* and Ω

In summary, the NRMS error results show that the different machine learning algorithms perform better after adding the Ω signal, and the NN performs more outstandingly, although it takes longer time to train the samples. In considering the real-time performance in actual application, the GBM, which takes longer, is also around 0.04s from the test time, while the time required for NN, RF is around 0.001s order of magnitude, so it satisfies the real-time performance requirement.

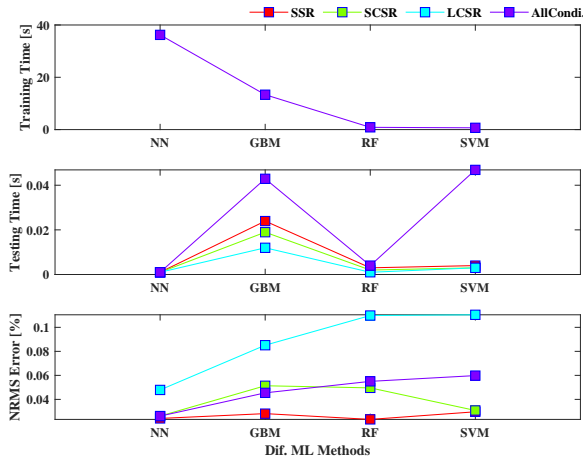


Fig. 25: Performance comparison of different ML methods using *AccZ* and Ω

Through the analysis and comparison, among the two input categories, the performance after adding V_w is more promising, so it is chosen for further analysis. In order to compare the

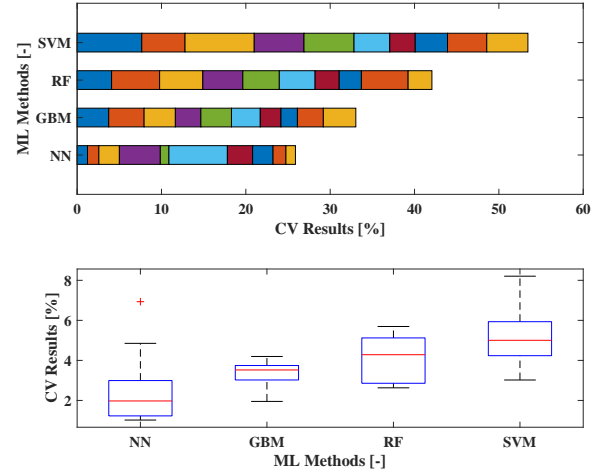


Fig. 26: CV Results of Different ML Methods

estimation results of these four machine learning algorithms better, a 10-fold CV of the AllCondi test set is performed to evaluate the performance of the algorithms more convincingly. This section will be expanded in the next subsection.

C. 10-folds CV using Ω and *AccZ*

To effectively test the performance of different machine learning algorithms on unknown data, an approach, k-fold cross-validation, is recommended. It is to split the training set data into k subsamples, keep one as the model test set data, and the remaining k-1 subsamples are used to train the model. k-fold CV is repeated so that each subsample can be sufficiently utilized. And that method is usually the most commonly used.

TABLE II: 10-Fold CV Performance

| Folds | NRMS error (%) | | | |
|-------|----------------|------|------|------|
| | NN | GBM | RF | SVM |
| 1 | 1.23 | 3.74 | 4.08 | 7.66 |
| 2 | 1.35 | 4.20 | 5.69 | 5.13 |
| 3 | 2.43 | 3.71 | 5.12 | 8.21 |
| 4 | 4.85 | 3.02 | 4.74 | 5.90 |
| 5 | 1.02 | 3.63 | 4.33 | 5.93 |
| 6 | 6.93 | 3.42 | 4.24 | 4.24 |
| 7 | 2.99 | 2.45 | 2.86 | 3.02 |
| 8 | 2.42 | 1.95 | 2.63 | 3.83 |
| 9 | 1.53 | 3.07 | 5.54 | 4.65 |
| 10 | 1.13 | 3.85 | 2.82 | 4.88 |
| Mean | 2.59 | 3.30 | 4.21 | 5.34 |

Table II shows the 10-fold CV results of the four algorithms, and the results of NN are better in terms of average value. The CV results are graphically illustrated for further analysis, as shown in Figure 26 for the stacked cubic plot and boxplot, respectively. The cumulative NRMS error is significantly larger for SVM, next to RF, GBM, and NN from the stacked cubic plot. it can be observed through also that the NRMS error value for the 6th (light blue) CV of NN is very remarkable, which may be the result of the LCSR working condition for a certain section of large slip ratio related to the *AccZ* anomaly, which should be the same sample as the anomalous value in Figure 18. It can be seen from the boxplot that the variance of GBM is the smallest, indicating the best stability. Although

the average is slightly larger than NN, the average of NN is the smallest, but there is an outlier. Although the performance of the two is more promising, Has its relatively complex model and quite long running time. The overall results of both RF and SVM are a bit worse, but both have less algorithm parameters and less time spent on training and testing samples.

VI. CONCLUSION

In this thesis, an intelligent tire system is tested on the MTS tire test bench to acquire acceleration signals under different longitudinal slip conditions. Then, the *AccZ* signal within the tire contact patch is extracted for filtering and used as inputs for the four machine learning algorithms, while Ω and *AccZ* are taken as inputs for the algorithms for comparative analysis. The results indicate that the performance of the latter is more promising. In order to evaluate the model performance of the four machine learning algorithms, the 10-fold CV method is performed for each of them. From the NRMS error results, the mean value of GBM is 3.30% and has the minimum variance, indicating better stability but more complicated models, the mean value of NN is 2.59% but has an outlier of 6.93%, and the mean values of RF and SVM algorithms are 4.21% and 5.34%, respectively, which have relatively inferior performance, but both have more simple models. In summary, the utilization of data from intelligent tire systems combined with machine learning algorithms has a high potential in the field of tire slip ratio estimation. For future research work, we will extend more training samples (for different tire brands, tire pressures, and even combined working conditions) to prove the performance of the intelligent tire system for slip ratio estimation.

REFERENCES

- [1] J. H. Park and C. Y. Kim, "Wheel slip control in traction control system for vehicle stability," *Vehicle system dynamics*, vol. 31, no. 4, pp. 263–278, 1999.
- [2] W.-Y. Wang, I.-H. Li, M.-C. Chen, S.-F. Su, and S.-B. Hsu, "Dynamic slip-ratio estimation and control of antilock braking systems using an observer-based direct adaptive fuzzy-neural controller," *IEEE Transactions on Industrial Electronics*, vol. 56, no. 5, pp. 1746–1756, 2008.
- [3] E. Liebmenn, K. Meder, J. Schuh, and G. Nenninger, "Safety and performance enhancement: The bosch electronic stability control (esp)," SAE Technical Paper, Tech. Rep., 2004.
- [4] Y. Hori, "Future vehicle driven by electricity and control-research on four wheel motored" uot electric march ii," in *7th International Workshop on Advanced Motion Control. Proceedings (Cat. No. 02TH8623)*. IEEE, 2002, pp. 1–14.
- [5] H. Heidfeld, M. Schünemann, and R. Kasper, "Ukf-based state and tire slip estimation for a 4wd electric vehicle," *Vehicle System Dynamics*, vol. 58, no. 10, pp. 1479–1496, 2020.
- [6] S. Seyedtabaai and A. Velayati, "Adaptive optimal slip ratio estimator for effective braking on a non-uniform condition road," *Automatika*, vol. 60, no. 4, pp. 413–421, 2019.
- [7] M. Boisvert and P. Micheau, "Estimators of wheel slip for electric vehicles using torque and encoder measurements," *Mechanical Systems and Signal Processing*, vol. 76, pp. 665–676, 2016.
- [8] H. Guan, B. Wang, P. Lu, and L. Xu, "Identification of maximum road friction coefficient and optimal slip ratio based on road type recognition," *Chinese Journal of Mechanical Engineering*, vol. 27, no. 5, pp. 1018–1026, 2014.
- [9] B.-R. Liang and W.-S. Lin, "A new slip ratio observer and its application in electric vehicle wheel slip control," in *2012 IEEE International Conference on Systems, Man, and Cybernetics (SMC)*. IEEE, 2012, pp. 41–46.
- [10] T. Vo-Duy and M. C. Ta, "Slip ratio estimation for traction control of electric vehicles," in *2018 IEEE Vehicle Power and Propulsion Conference (VPPC)*. IEEE, 2018, pp. 1–6.
- [11] Y. Zhang, H. Zhao, L. Yuan, and H. Chen, "Slip ratio estimation for electric vehicle with in-wheel motors based on ekf without detection of vehicle velocity," in *2016 Chinese Control and Decision Conference (CCDC)*. IEEE, 2016, pp. 4427–4432.
- [12] K. Maeda, H. Fujimoto, and Y. Hori, "Four-wheel driving-force distribution method based on driving stiffness and slip ratio estimation for electric vehicle with in-wheel motors," in *2012 IEEE Vehicle Power and Propulsion Conference*. IEEE, 2012, pp. 1286–1291.
- [13] M. Cecotti, J. Larminie, and B. Azzopardi, "Estimation of slip ratio and road characteristics by adding perturbation to the input torque," in *2012 IEEE International Conference on Vehicular Electronics and Safety (ICVES 2012)*. IEEE, 2012, pp. 31–36.
- [14] K. Fujii and H. Fujimoto, "Traction control based on slip ratio estimation without detecting vehicle speed for electric vehicle," in *2007 Power Conversion Conference-Nagoya*. IEEE, 2007, pp. 688–693.
- [15] S. Antonov, A. Fehn, and A. Kugi, "Unscented kalman filter for vehicle state estimation," *Vehicle System Dynamics*, vol. 49, no. 9, pp. 1497–1520, 2011.
- [16] L.-Y. Hsu and T.-L. Chen, "Vehicle full-state estimation and prediction system using state observers," *IEEE Transactions on Vehicular Technology*, vol. 58, no. 6, pp. 2651–2662, 2008.
- [17] L. Imsland, T. A. Johansen, T. I. Fossen, H. F. Grip, J. C. Kalkkuhl, and A. Suissa, "Vehicle velocity estimation using nonlinear observers," *Automatica*, vol. 42, no. 12, pp. 2091–2103, 2006.
- [18] K. Guo and D. Lu, "Unifit: unified tire model for vehicle dynamic simulation," *Vehicle System Dynamics*, vol. 45, no. S1, pp. 79–99, 2007.
- [19] H. B. Pacejka and E. Bakker, "The magic formula tyre model," *Vehicle system dynamics*, vol. 21, no. S1, pp. 1–18, 1992.
- [20] H. Lee and S. Taheri, "A novel approach to tire parameter identification," *Proceedings of the Institution of Mechanical Engineers, Part D: Journal of Automobile Engineering*, vol. 233, no. 1, pp. 55–72, 2019.
- [21] N. Xu, H. Askari, Y. Huang, J. Zhou, and A. Khajepour, "Tire force estimation in intelligent tires using machine learning," *IEEE Transactions on Intelligent Transportation Systems*, pp. 1–10, 2020.
- [22] N. Xu, Y. Huang, H. Askari, and Z. Tang, "Tire slip angle estimation based on the intelligent tire technology," *IEEE Transactions on Vehicular Technology*, vol. 70, no. 3, pp. 2239–2249, 2021.
- [23] D. Maurya, S. Khaleghian, R. Sriramdas, P. Kumar, R. A. Kishore, M. G. Kang, V. Kumar, H.-C. Song, S.-Y. Lee, Y. Yan *et al.*, "3d printed graphene-based self-powered strain sensors for smart tires in autonomous vehicles," *Nature communications*, vol. 11, no. 1, pp. 1–10, 2020.
- [24] H. Askari, E. Hashemi, A. Khajepour, M. B. Khamesee, and Z. L. Wang, "Tire condition monitoring and intelligent tires using nanogenerators based on piezoelectric, electromagnetic, and triboelectric effects," *Advanced Materials Technologies*, vol. 4, no. 1, p. 1800105, 2019.
- [25] Askari, Hassan and Hashemi, Ehsan and Khajepour, Amir and Khamesee, Mir Behrad and Wang, Zhong Lin, "Towards self-powered sensing using nanogenerators for automotive systems," *Nano Energy*, vol. 53, pp. 1003–1019, 2018.
- [26] A. J. Tuononen, "Optical position detection to measure tyre carcass deflections," *Vehicle System Dynamics*, vol. 46, no. 6, pp. 471–481, 2008.
- [27] R. Matsuzaki and A. Todoroki, "Wireless flexible capacitive sensor based on ultra-flexible epoxy resin for strain measurement of automobile tires," *Sensors and Actuators A: Physical*, vol. 140, no. 1, pp. 32–42, 2007.
- [28] F. Coppo, G. Pepe, N. Roveri, and A. Carcatera, "A multisensing setup for the intelligent tire monitoring," *Sensors*, vol. 17, no. 3, p. 576, 2017.
- [29] A. Pohl, R. Steindl, and L. Reindl, "The" intelligent tire" utilizing passive saw sensors measurement of tire friction," *IEEE transactions on instrumentation and measurement*, vol. 48, no. 6, pp. 1041–1046, 1999.
- [30] O. Yilmazoglu, M. Brandt, J. Sigmund, E. Genc, and H. Hartnagel, "Integrated inas/gasb 3d magnetic field sensors for "the intelligent tire"," *Sensors and Actuators A: Physical*, vol. 94, no. 1-2, pp. 59–63, 2001.
- [31] V. Magori, V. R. Magori, and N. Seitz, "On-line determination of tyre deformation, a novel sensor principle," in *1998 IEEE Ultrasonics Symposium. Proceedings (Cat. No. 98CH36102)*, vol. 1. IEEE, 1998, pp. 485–488.
- [32] H. Lee and S. Taheri, "Intelligent tires? a review of tire characterization literature," *IEEE Intelligent Transportation Systems Magazine*, vol. 9, no. 2, pp. 114–135, 2017.
- [33] H.-N. Robert *et al.*, "Theory of the backpropagation neural network," *Proc. 1989 IEEE IJCNN*, vol. 1, pp. 593–605, 1989.

- [34] J. H. Friedman, “Greedy function approximation: a gradient boosting machine,” *Annals of statistics*, pp. 1189–1232, 2001.
- [35] T. K. Ho, “The random subspace method for constructing decision forests,” *IEEE transactions on pattern analysis and machine intelligence*, vol. 20, no. 8, pp. 832–844, 1998.
- [36] W. S. Noble, “What is a support vector machine?” *Nature biotechnology*, vol. 24, no. 12, pp. 1565–1567, 2006.



Nan Xu received the Ph.D. degree in vehicle engineering from Jilin University, Changchun, China, in 2012. He is currently an associate professor at State Key Laboratory of Automotive Simulation and Control, Jilin University. His current research focuses on tire dynamics, intelligent tire, vehicle dynamics, stability control of electric vehicles and autonomous vehicles.



Zepeng Tang is currently a M.S. candidate in the College of Automotive Engineering, Jilin University, Changchun, China. His research interest is mainly on intelligent tire, vehicle dynamics and autonomous vehicles.



Jianfeng Zhou received his B.E. degree in automotive engineering in 2018 from Jinlin University, Changchun, China, where he is currently working toward the M.S. degree. His current research focuses on tire dynamics, intelligent tire and vehicle dynamics.



Hassan Askari was born in Rasht, Iran and received his B. Sc., M.Sc. and PhD degrees from Iran University of Science and Technology, Tehran, Iran, University of Ontario Institute of Technology, Oshawa, Canada, and University of Waterloo, Waterloo, Canada in 2011, 2014, and 2019 respectively. He published more than 70 journal and conference papers in the areas of nonlinear vibrations, applied mathematics, nanogenerators and self-powered sensors. He co-authored one book and one book chapter both published by Springer. He is an active reviewer

for more than 40 journals and editorial board member of several scientific and international journals. He has received several prestigious awards including, Outstanding Researcher at the Iran University of Science and Technology, Fellowship of the Waterloo Institute of Nanotechnology, NSERC Graduate Scholarship, Ontario Graduate Scholarship, and the University of Waterloo President Award. He was nominated for the Governor General’s Academic Gold Medal at the University of Ontario Institute of Technology and University of Waterloo in 2014 and 2019, respectively. He is currently a Postdoctoral Fellow at the Department of Mechanical and Mechatronics Engineering at the University of Waterloo.